Characterization of Shortwave Fadeout seen in Daytime SuperDARN Ground-Scatter Observations

S. Chakraborty, J. M. Ruohoniemi, J. B. H. Baker

Department of Electrical and Computer Engineering, Virginia Tech, Blacksburg, VA, USA

Space @ Virginia Tech — Center for Space Science and Engineering Research

Virginia Tech — Invent the Future®

Abstract

Shortwave fadeout (SWF) is one of the well-known radio wave anomalies that occur in the upper atmosphere. During a solar flare, the sun emits soft and hard X-rays in the order of ≤1 nm, which penetrate through the ionosphere and reach the D-layer, resulted in a sudden increase in plasma density. This sudden enhancement in plasma density increases the attenuation of radio waves. SWF causes disruption on HF communication channels that persists for 10's of minutes to a few hours. SuperDARN observations of daytime ground-scatter are strongly affected; the average number of ground-scatter echoes drops suddenly (≈1 min) and often reaches to zero. Ground-scatter echoes not only experience absorption but also undergo a sudden phase change [Watanabe et al. 2013] that leads to an apparent, brief increase in ground-scatter velocity, resulted in a 'velocity flash' feature. We have analyzed a number of events and report here on the characteristics of SWF in SuperDARN observations produced by M and X-class solar flares. The first effect of SWF is usually the velocity flash which lasts only a few 10s of seconds. Then the average number of ground-scatter echoes starts to decrease sharply marking an onset and leads to a blackout phase. During the blackout phase the ground-scatter is typically suppressed for 10s of minutes, and then it recovers back to pre-SWF echo-count through the recovery phase over half an hour. The intensity of SWF effect seen in SuperDARN ground-scatter depends on the solar zenith angle and operating frequency of the radar. In this presentation, we discuss the basic characteristics of SWF events seen in SuperDARN radar observations and different parameters which control the intensity of the event and the effect ionospheric dynamics during SWF. We also describe a Python-based tool that can monitor the ground-scatter observations and detects SWF across North America, using the network of SuperDARN radars.

Introduction

❑ The quiet Sun emits EM radiation in all possible frequency spectrum; among these frequency bands EUV spectrum is responsible for the formation of ionosphere. Higher energetic cosmic radiations penetrate much lower in the atmosphere (almost to the D-layer of ionosphere, $70 \leq h \leq 90\ km$). During a solar flare event, the spectral irradiance of X-ray band enhances many folds ($\approx 10 - 1000$ times), which enhances D-region ionization on the day side dramatically, leads to bending in radio waves due to change in refractive index of the D-layer, and an increase in radio wave absorption. This sudden increase of plasma density following a solar flare event produces a sudden increase in radio-wave absorption that is most severe in the high frequency (HF) ranges, commonly known as ShortWave Fadeout (SWF), which is the earliest space weather effect. SuperDARN observations of daytime ground-scatter are known to be strongly affected by SWF. We used mid and high latitude SuperDARN radar chain across North America to study the basic characterization and timing analysis of SWF. Figure 1 shows the locations of the SuperDARN radars, which are used in this study.

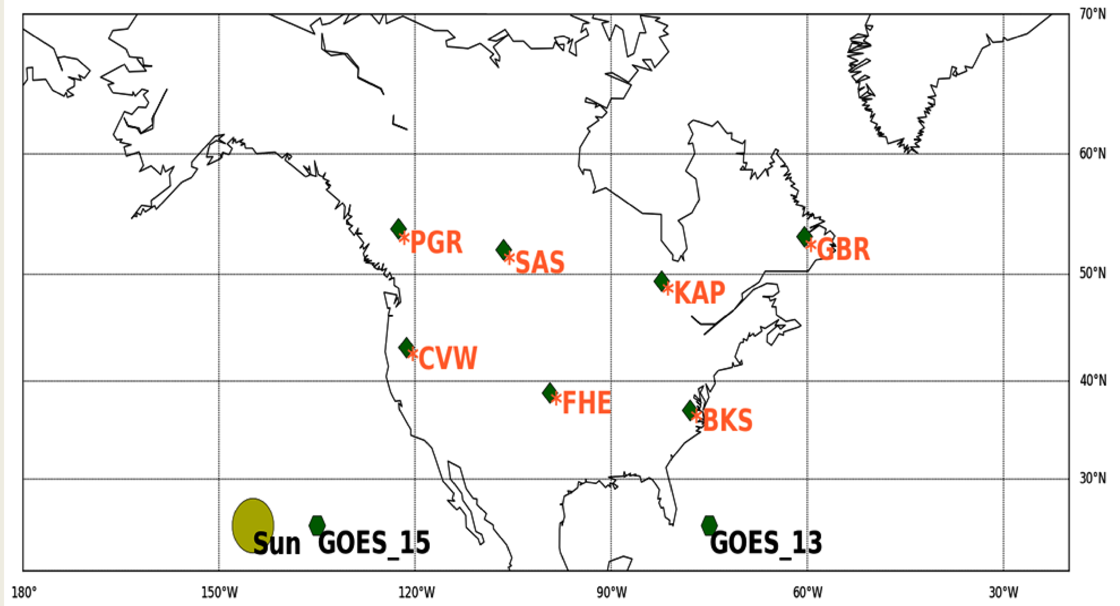

Figure 1: Mid and high latitude SuperDARN radars (across North America) used to monitor Shortwave Fadeout. Mid-latitude radars – BKS,FHE,CVW; High-latitude radars – GBR, KAP, SAS, PGR.

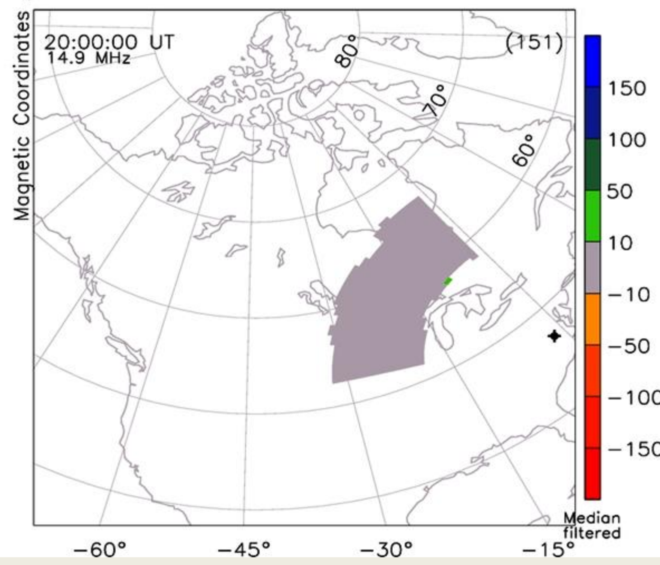

Figure 2: Stable daytime ground-scatter echoes observed (marked in grey) in SuperDARN radar.

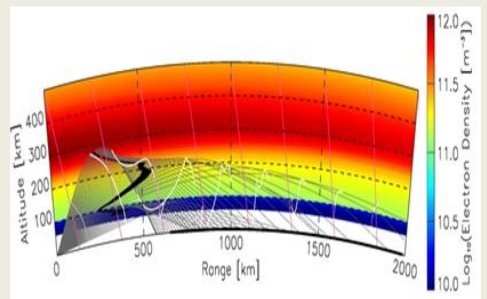

Figure 3: Ground-scatter simulates a 2-way OTH ground to ground communication link.

Observations

❑ Figure 2 & 3 gives an shows that SuperDARN daytime observations are populated by the ground-scatter. Doppler velocity and spectral width of SuperDARN ground-scatters echoes are smaller than that of ionospheric echoes. Doppler velocity of ground-scatter is less than $\pm 10\ m/s$. However Figure 4 presents variations in velocity and strength of ground-scatter observation during an SWF [*Watanabe et. al., 2013*].

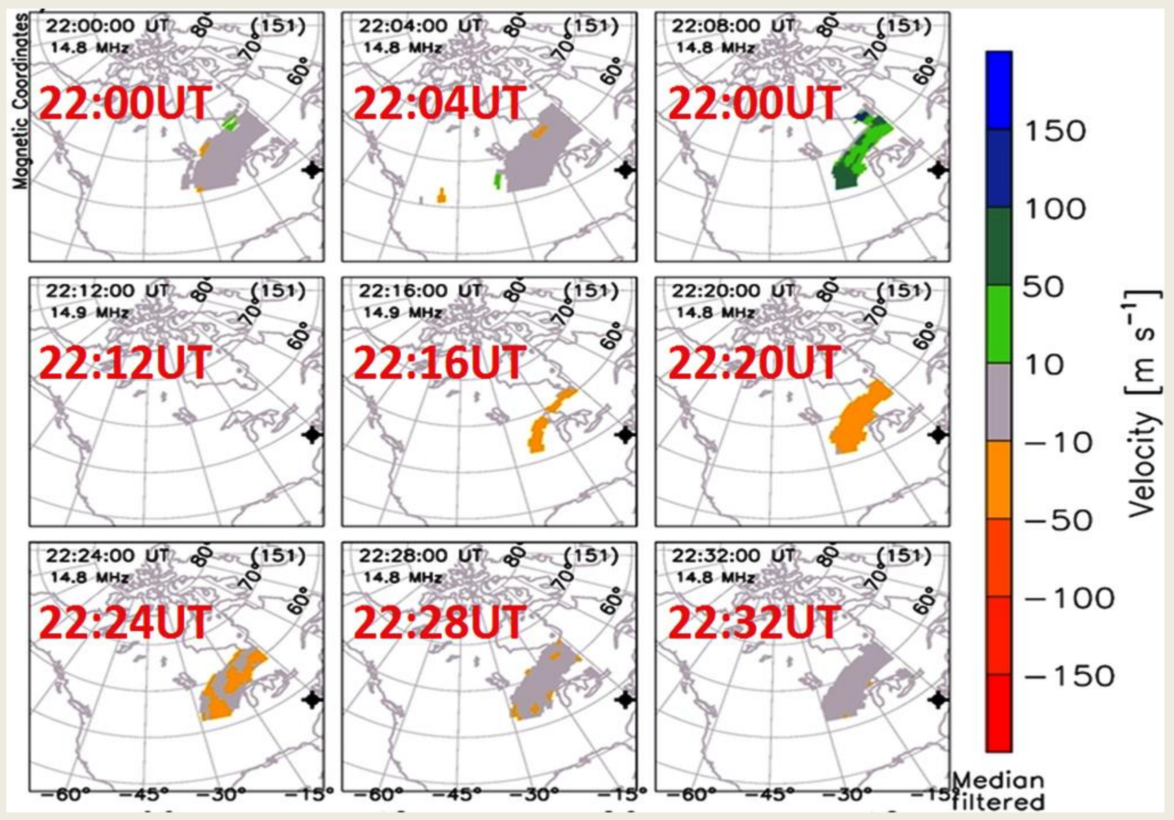

Figure 4: Field-of-view (FoV) plot of a SuperDARN radar during an SWF event on $5^{th} May, 2015\ at\ 22{:}10\ UT$. Each panel is a snapshot of radar scan taken at different time during the event.

❑ Figure 5 presents different phases ***(onset, blackout and recovery)*** of SWF event seen in ground-scatter observation. It also shows the time evolution of travelling radio wave attenuation due to SWF.

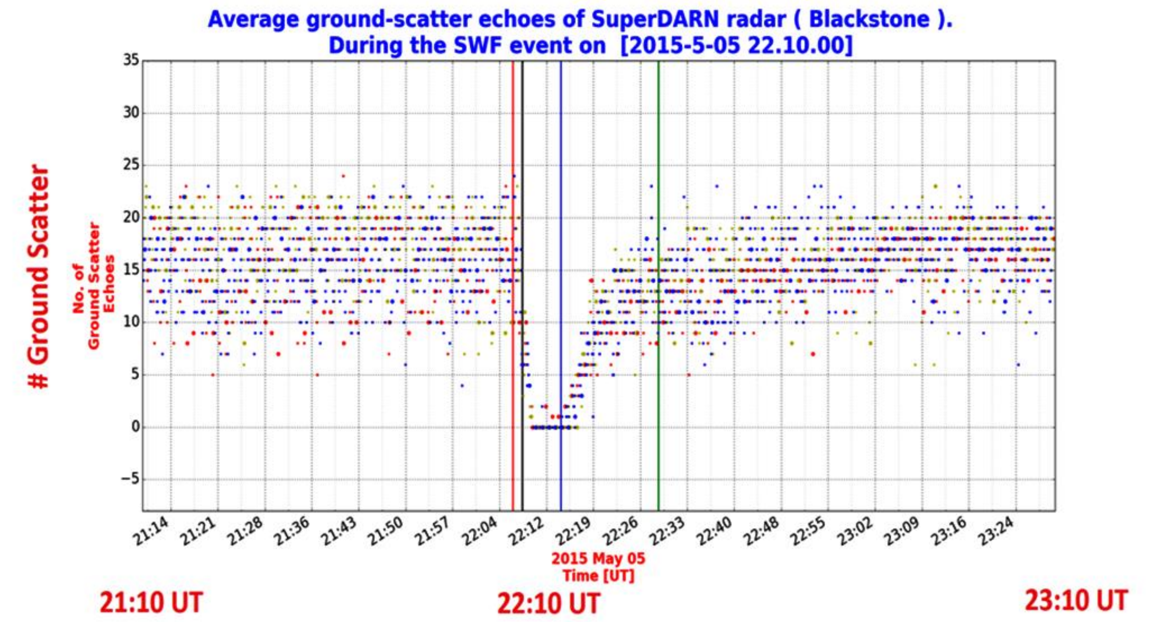

Figure 5: Different phases of SWF. Vertical lines are the demarcation between phases. Red line is centered start of onset, black line is start of max absorption, blue line is end of max absorption and green line is recovery.

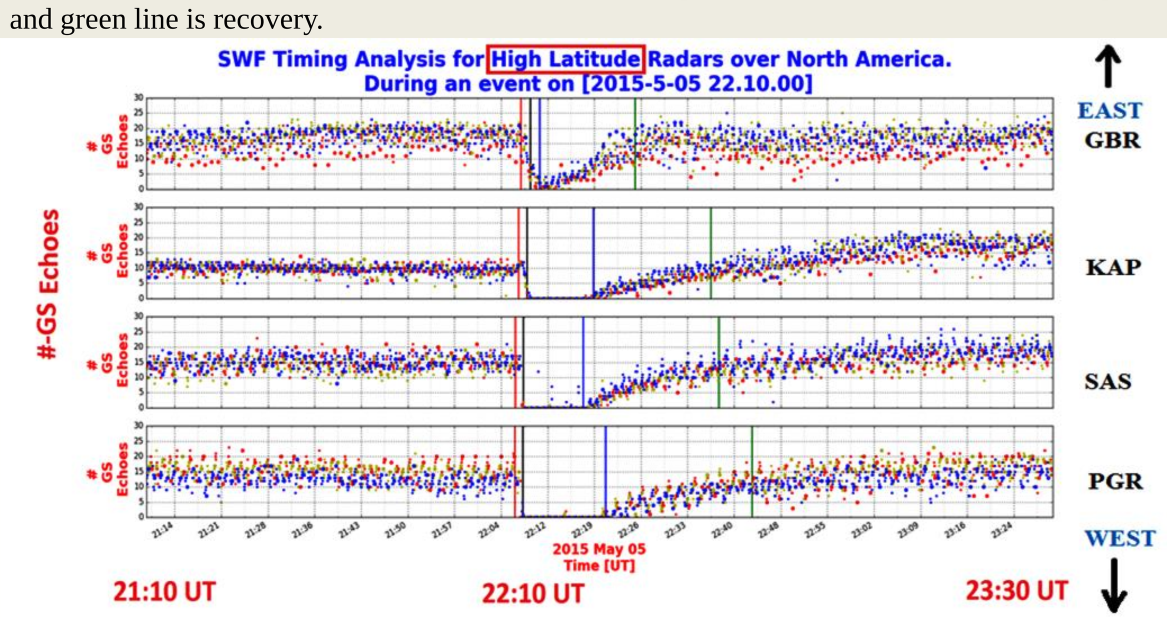

Figure 6: Stack plot of average ground-scatter echoes timing analysis. Radars are sorted as decrease in solar zenith angle (top-down). During this particular event (on $5^{th} May, 2015\ at\ 22{:}10\ UT$) Sun was due West.

Observations (cont.)

❑ Figure 6 shows a clear progression in different phase timings and intensity of absorption from East to West. For this event, the sub-solar point was over Pacific ocean as shown in Figure 1, so, western radars are more affected by the SWF.

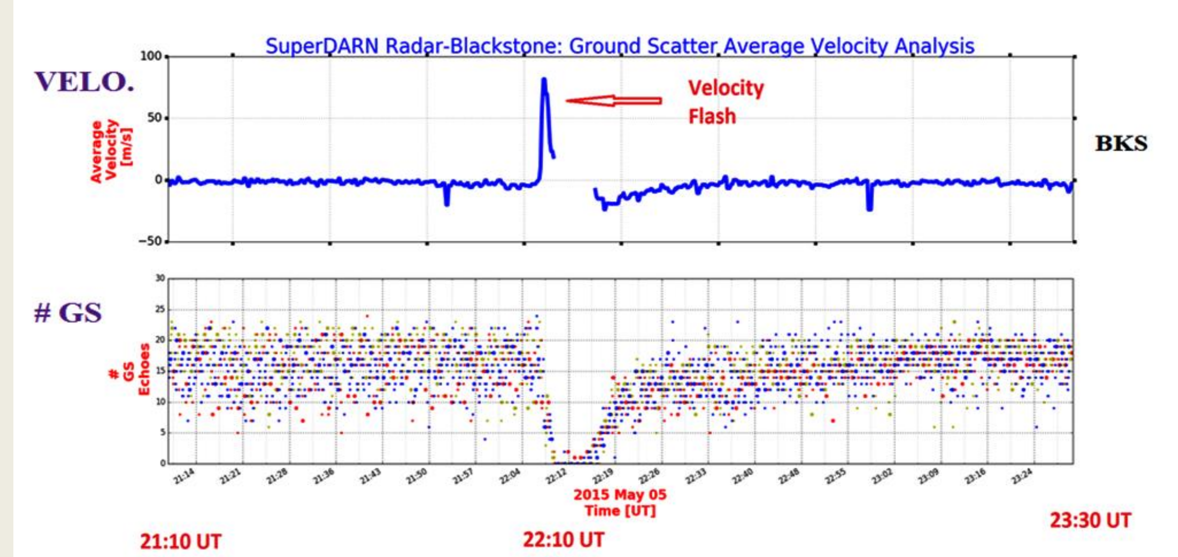

Figure 7: Sudden enhancement in ground-scatter velocity just before . Stack plot of average ground-scatter echoes timing analysis. Radars are sorted as decrease in solar zenith angle (top-down). During this particular event (on $5^{th} May, 2015\ at\ 22{:}10\ UT$) Sun was due West.

❑ Daytime ground-scatter observation of SuperDARN radars often undergoes a velocity flash during an SWF event. Just like onset phase of the SWF in ground-scatter observation, it's also a precursor to the event.

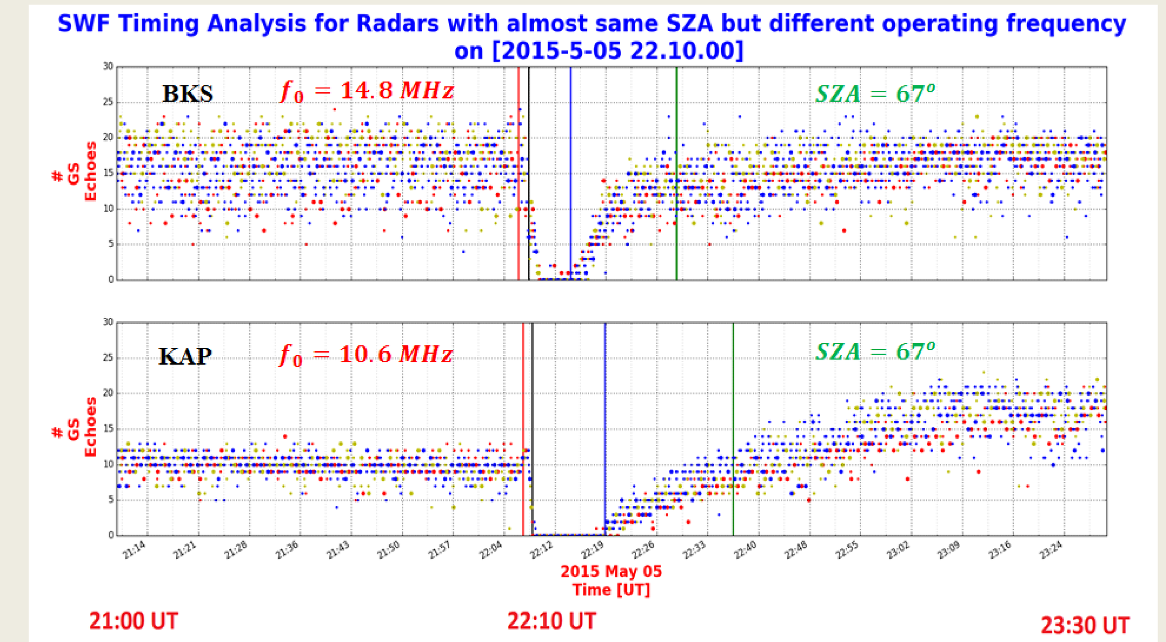

Figure 8: Compare timings of SWF phases for the radars with different operating frequency . Stack plot of average ground-scatter echoes timing analysis. Radars are sorted as decrease in solar zenith angle (top-down). During this particular event (on $5^{th} May, 2015\ at\ 22{:}10\ UT$) Sun was due West.

❑ Figure 8 shows a comparison of SWF intensity on radio wave having different frequency. It's certain that, radar having relatively less operating frequency (bottom panel) is more affected by the event.

❑ Figure 9 presents statistical results of onset phase duration. This study shows that average duration of onset phase is approximately 1-2 minutes, which is typically one scan time of radar. So, this proves that onset of SWF event is sudden and sharp.

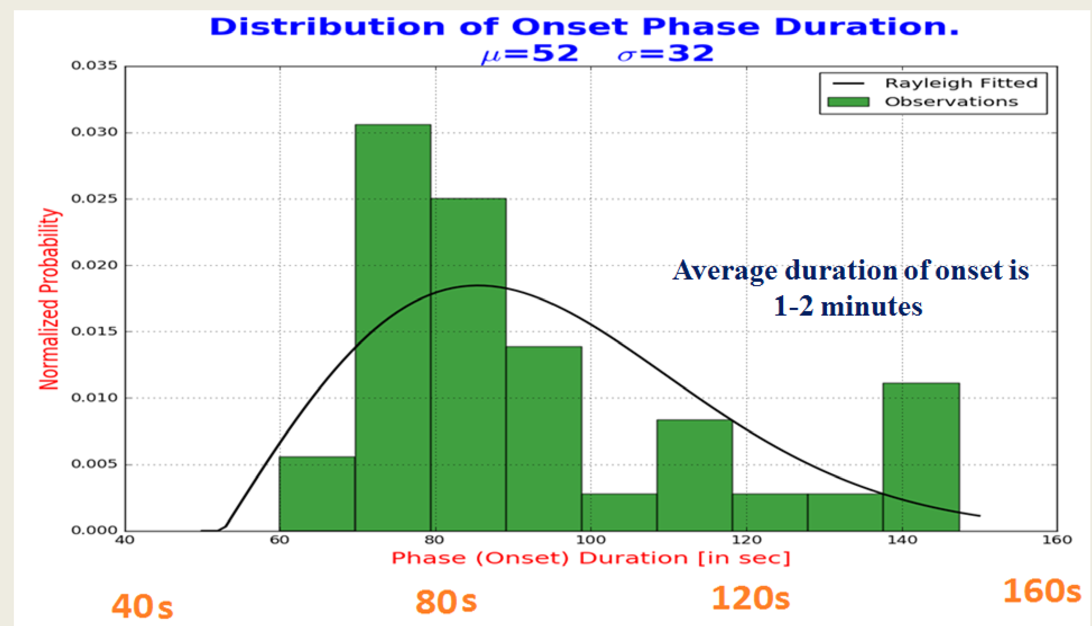

Figure 9: Average onset phase duration. Statistical result shows average onset duration of SWF event is 1-2 minutes.

Autonomous Tools

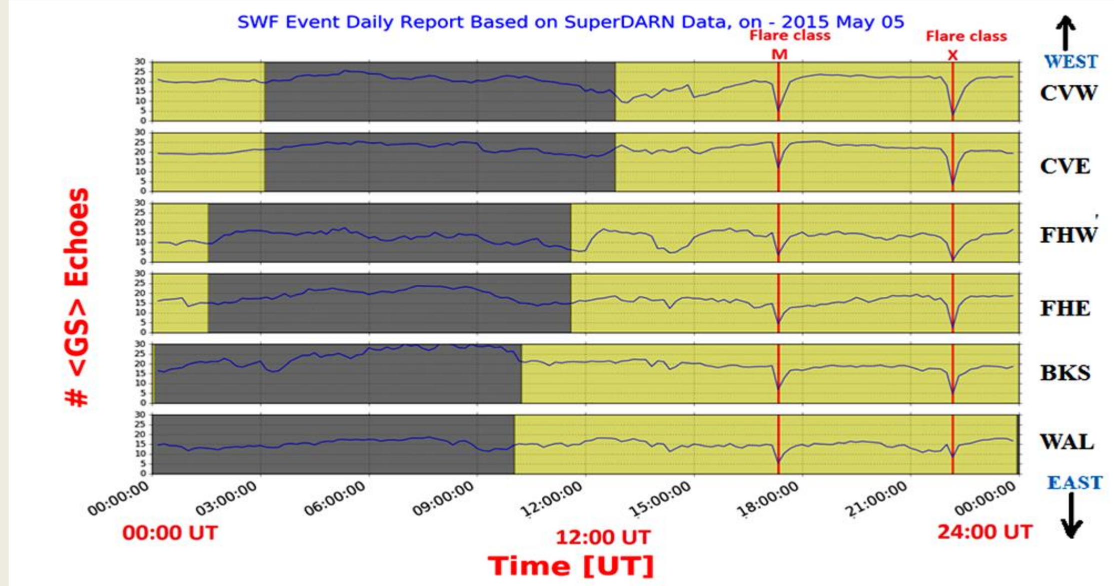

Figure 10: Automated SWF event Detection – Daily Summary Report

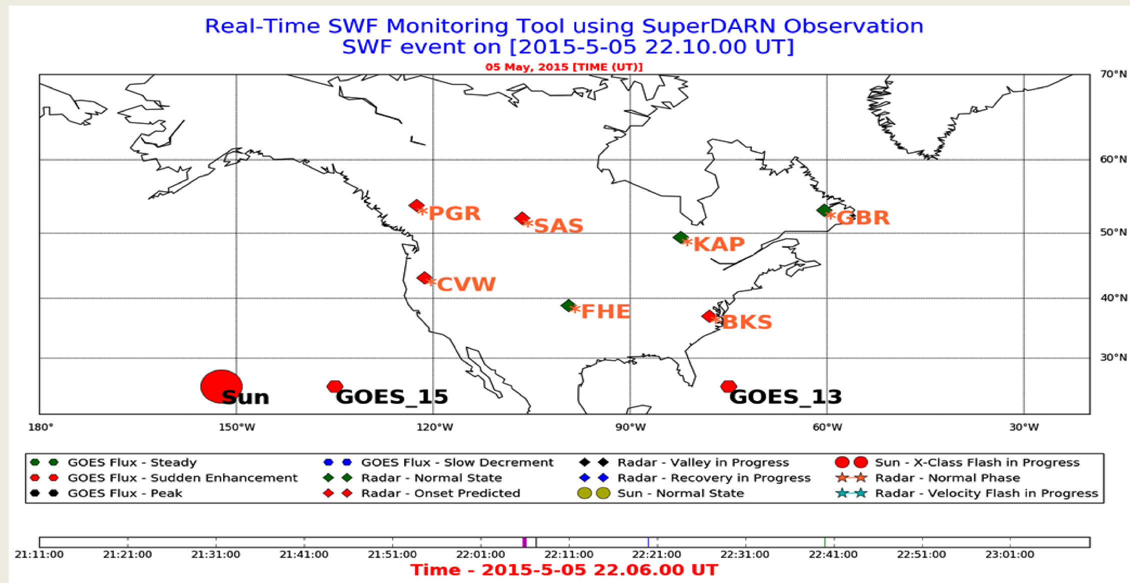

Figure 11: Snapshot of real-time SWF monitoring tool. Onset is in progress.

❑ Figure 10 shows output of a SWF detection tool. This tool can go through the SuperDARN database and detects occurrence and time of the SWF in the SuperDARN observation. It uses the characterization methods to detect SWF.

❑ Figure 11 is the outputs of real-time SWF monitoring tool. This tool monitors SWF events. It uses the SuperDRAN daytime ground-scatter observations of the radar chain deployed across North America to monitor progression of SWF across the continent. Tool notifies different phases by changing colors of the radar sites.

Conclusions

❑ We characterize SWF events based on depth of blackout and duration of the event phases seen in SuperDARN ground-scatter observations.

❑ We see suppression in ground scatter during the main phase of the event, which is antecedent by a sudden increase in velocity. This velocity flash is acting as a precursor of SWF event.

❑ Automated event detection tool is used to search SWF patterns in SuperDARN database. On the other hand real-time SWF monitoring tool is used to monitor progression of SWF across North America. Both the tools use the knowledge of SWF characterization seen in SuperDARN observation.

❑ Future work : A web-based real-time SWF monitoring tool is in development.

References

❑ NOAA, Global D-Region Absorption Prediction Documentation, http://www.swpc.noaa.gov/content/global-d-region-absorption-prediction-documentation 2015.

❑ H.H. Sauer, Global mapping of ionospheric HF/VHF radio wave absorption due to solar energetic protons, American Geophysical Union: Space Weather, 2008.

❑ NOAA, DRAP ModelValidation: I. Scientific Report, https://www.ngdc.noaa.gov/stp/drap/DRAP-V-Report1.pdf, 2010.

❑ Daiki Watanabe, Study of ionospheric disturbances during solar flare events using the SuperDARN Hokkaido radar, 2013.

Contact: *shibaji7@vt.edu*

S.Chakraborty is funded by NSF